

Analysis of Correlation Between Flexural Strength and Pore Characteristics on CFRP Rebar by Fabrication Method

Nam-II Kim, Do-Young Kwon, Yong-Sik Chu*

Carbon Neutral Material Center, Korea Institute of Ceramic Eng. and Tech.

*Corresponding author: Yong-Sik Chu, yschu@kicet.re.kr

Copyright: © 2023 Author(s). This is an open-access article distributed under the terms of the Creative Commons Attribution License (CC BY 4.0), permitting distribution and reproduction in any medium, provided the original work is cited.

Abstract

In this study, the fabrication conditions of carbon fiber reinforced polymer (CFRP) rebar were controlled to derive the correlation between flexural strength and pore characteristics. The fabrication conditions of CFRP rebar were adjusted for presence or absence of rib, resin temperature, and curing furnace temperature. Flexural strength and pore characteristics of fabricated CFRP rebar were analyzed. The flexural strength of CFRP rebar was changed depending on the fabrication condition, such as the presence or absence of rib, the resin temperature, and the curing furnace temperature. It was confirmed that the flexural strength of CFRP rebar was significantly lowered when the rib was not wound. As a result of Nano X-ray computed tomography (CT) analysis, the maximum pore diameter was shown in CFRP rebar prepared at a resin temperature of 60°C. According to optical microscopic analysis, the maximum porosity was 6.89% in No. 1, and the minimum porosity was 2.88% in No. 7. The correlation coefficient between porosity and flexural strength using optical microscopy was -0.64, which was higher than the correlation coefficient between porosity and pore size using Nano X-ray CT.

Keywords

Flexural strength
Porosity
Resin temperature
Rib
Correlation coefficient

1. Introduction

Reinforcing steel has been widely used to strengthen concrete structures due to its excellent elastic, ductile, and plastic properties^[1-3]. However, the use of rebar in coastal areas is limited by corrosion, which reduces the

service life of the structure^[4,5]. In addition, corrosion of rebar by snow removal agents increases the cost of rehabilitation of the structure. In recent years, with the continuous development of aviation, automotive, marine, and construction industries, and advances in technology,

research on the development of new materials with lightweight, high strength, and non-corrosive properties has been actively conducted [6-12]. Among them, fiber reinforced polymer (FRP) composites have been actively used as a substitute for metal materials. In the construction industry, FRP rebars have been newly researched and applied as a substitute for corrosion prevention of rebar [13-15]. In particular, FRP rebars have excellent tensile stiffness, light weight, and durability, and have already been applied to some concrete structures. However, FRP rebars lack ductility, which means that the stress and strain remain linear until the maximum load is reached. Many studies have been conducted on the flexural strength characteristics of concrete using FRP rebars, and it has been reported that the flexural strength of concrete is significantly improved [16,17]. In addition, some researchers have examined the mixed use of steel bars to improve the disadvantages of FRP rebars with low ductility [18]. In addition, research on composite steel (core) and FRP (surface) to maintain the advantage of ductility of steel bars has also been promoted [19].

The flexural strength properties of FRP composites have been studied by some researchers. However, most of the studies were conducted on the bending strength of cuboidal shapes made by lay-up method rather than pultruded bar shape [20]. Therefore, the manufacturing method and shape of existing FRP composites are completely different from steel bars (round or deformed), and it is difficult to accurately evaluate the flexural strength characteristics of FRP rebars. In other words, there are very few studies on the flexural strength characteristics of FRP rebars with rebar shapes, and in particular, there are no studies on the correlation between the flexural strength and porosity of carbon fiber reinforced polymer (CFRP) rebars.

Therefore, in this study, various manufacturing conditions were examined to determine the flexural strength of CFRP rebars, and the pore content and size of CFRP rebars were analyzed to derive the correlation with the flexural strength. In particular, to identify the

pore characteristics of CFRP rebars, X-ray computed tomography (CT) imaging for three-dimensional shape and characterization, and optical microscopy observation and image analysis for cross-sectional characterization were performed.

2. Experimental method

In this study, CFRP rebars were manufactured using the pultrusion machine shown in **Figure 1**, and the polymer was a mixture of epoxy resin and curing agent from Kukdo Chemical. The fibers used were 24 K carbon fiber from Korea's H company and 4,400 TEX glass fiber from China's C company (carbon fiber for the CFRP rebar core and glass fiber for the ribs). The pultrusion machine used in this study consists of carbon fiber creel, resin impregnation bath, rib winding, curing furnace, and pultrusion machine, and CFRP rebar (5 mm diameter) was manufactured by controlling the resin temperature of the resin impregnation bath and the curing furnace temperature.

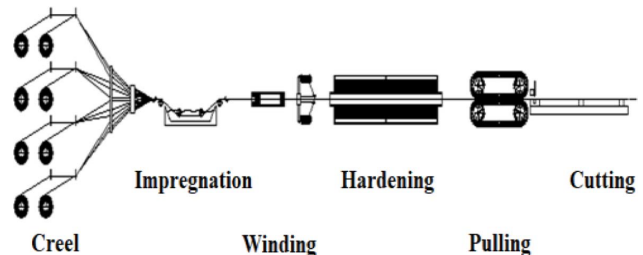


Figure 1. Schematic diagram of pultrusion machine for manufacturing CFRP rebar

The CFRP rebar manufacturing conditions are shown in **Table 1**, and the resin temperature was varied from 30°C to 60°C. The curing furnace was controlled from 100°C to 195°C in three sections. In particular, No. 1 shows the manufacturing condition without ribbing, and No. 2-7 show the CFRP manufacturing condition with ribbing. The appearance of the CFRP rebar produced by the pultrusion machine in **Figure 1** and the manufacturing conditions in **Table 1** is shown in **Figure 2**.

Table 1. Fabrication condition of CFRP rebar

No.*	Impregnation temperature (°C)	Hardening temperature (°C)			Pultrusion speed (cm/min)	Hardening time (min)
		1 area	2 area	3 area		
1	30	170	175	170	24	5
2	30	170	175	170	24	5
3	30	190	195	190	24	5
4	45	100	150	150	6	15
5	60	100	150	150	6	15
6	45	100	150	150	3	30
7	45	100	170	170	3	30

*No. 1: CFRP rebar without rib, No. 2–7: CFRP rebar with rib

An X-ray CT (Vtomex M 240D) from GE Sensing & Inspection Tech. (Germany) was used for three-dimensional characterization of the pultruded CFRP rebars according to the respective manufacturing conditions, and an optical microscope (DSXC-HRSU-RF) from Olympus (Japan) was used for cross-sectional pore characterization. 100-ton strength tester from Woojin Precision (Korea) was used to measure the flexural strength, and a Rigaku (Japan) TG-DTA 8122 thermal analyzer was used to measure the decomposition temperature of resins and fibers. Through the above analysis, the correlation between pore characteristics and flexural strength properties was derived.

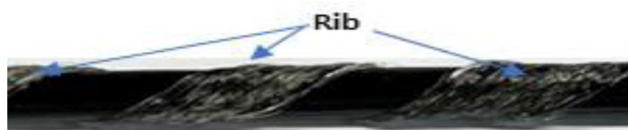


Figure 2. View of CFRP rebar

3. Results and discussion

3.1. Flexural strength properties

The results of the flexural strength measurements of CFRP rebars under different manufacturing conditions are shown in **Figure 3**. The flexural strength varied depending on the manufacturing condition, especially the presence or absence of ribs. No. 1 is a CFRP rebar without ribs and No. 2 is a CFRP rebar with wrapped ribs, and the flexural strength increased by about

25.6% (14.6 MPa to 18.3 MPa) when ribs were present. The flexural strength also increased from 16.3 MPa to 17.3 MPa when the resin temperature in the resin impregnation bath was increased from 45°C to 60°C. The flexural strength also increased with increasing curing temperature and curing time, and the best flexural strength properties (18.7 MPa) were obtained at a resin temperature of 45°C, a maximum curing temperature of 170°C, and a curing time of 30 minutes. **Table 2** shows the increase in flexural strength for each manufacturing condition, and the highest increase in strength was achieved with and without ribs. In addition, it was found that the flexural strength values of CFRP rebars varied with the presence or absence of ribs, curing temperature, curing time, and resin impregnation bath temperature.

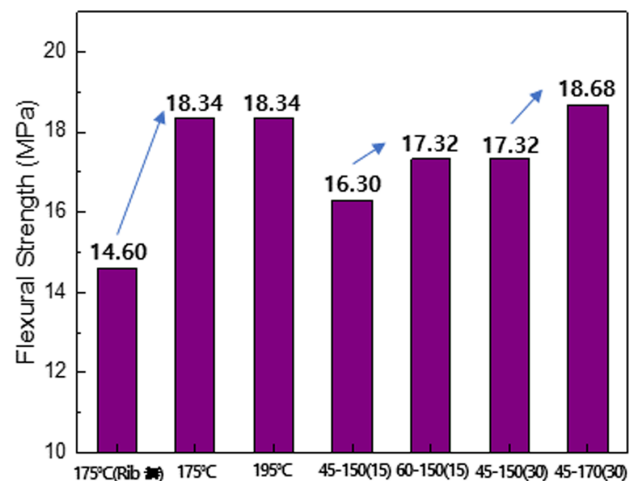


Figure 3. Flexural strength of CFRP rebar

Table 2. Flexural strength increase ratio as manufacturing conditions of CFRP rebar

Factor	Flexural strength (MPa)		Increase ratio (%)
	Before	After	
Rib	14.6	18.3	+25.6
Impregnation temperature	16.3	17.3	+6.3
Hardening temperature	17.3	18.7	+7.9
Hardening time	16.3	17.3	+6.3

Table 3. Maximum pore size and porosity obtained by X-ray CT analysis

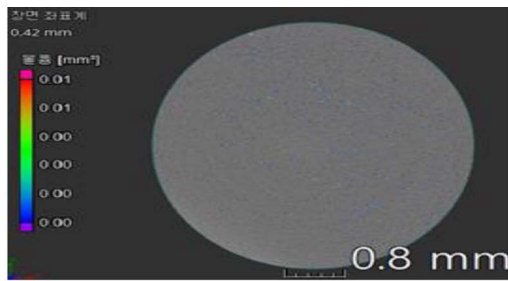
No.	Maximum pore volume (mm ³)	Maximum pore diameter (mm)	Porosity (%)
1	7×10^{-2}	0.51	2.47
2	1×10^{-2}	0.27	0.90
3	3.5×10^{-1}	0.87	1.05
4	1×10^{-3}	0.13	3.27
5	3.9×10^{-1}	0.91	1.49
6	7×10^{-4}	0.11	3.64
7	4×10^{-4}	0.09	3.22

3.2. Pore characterization

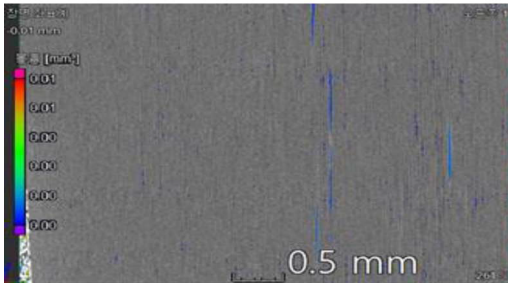
To analyze the three-dimensional structure of the CFRP rebar, X-ray CT measurements were taken with a diameter of 5 mm and a length of 10 mm. The X-ray CT analysis was performed on the longitudinal, cross-sectional, and three-dimensional structures of the CFRP rebars, and an example of an analysis photo (No. 2) is shown in **Figure 4**. Defects were observed in all CFRP rebars, and the color of the defect was different depending on the volume of the defect, i.e., red color for larger defect volume, and blue color for smaller defect volume. CFRP bar defects were observed in all parts of the bar, especially at the rib joints. For example, the pink and green areas observed in the lower left corner of the 3D image in **Figure 4(c)** are defects observed where the ribs are bonded. It was assumed that the defect was generated by absorption of resin from the main reinforcement (carbon fiber) impregnated with resin by the non-resin impregnated rib (glass fiber). In addition, the blue line and dotted line defects in the longitudinal section in **Figure 4(b)** or the green line and dotted line defects in the three-dimensional structure in **Figure 4(c)** are

defects that occur between the carbon fibers, which are believed to be caused by the failure of the fibers to bond perfectly during the bonding process of the carbon fibers impregnated in the resin impregnation bath. The above phenomena are typical of all CFRP rebars, not just No. 2.

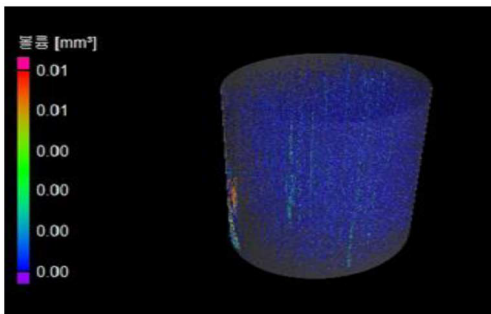
The defects with the largest volume among the defects observed in X-ray CT are shown in **Table 3**. The pore diameter was calculated by assuming the defect volume to be the volume of a spherical pore, and the percentage of the defect was expressed as the porosity ratio (hereafter, the defect is expressed as a pore). The maximum pore volume of CFRP bar (No. 1) without wrapped ribs was 0.07 mm³ with a diameter of 0.51 mm and a porosity of 2.47%. The sample with the largest pore diameter among the CFRP rebars was No. 5 (0.91 mm), and the resin temperature was increased to 60°C when manufacturing No. 5. As a result, the CFRP rebar experienced some curing phenomena after passing through the resin impregnation bath (before entering the curing furnace), and it was assumed that some of the large pores inside the CFRP rebar were not filled due to the abnormal curing phenomenon of the resin. In other



(a) Cross-section



(b) Longitudinal section

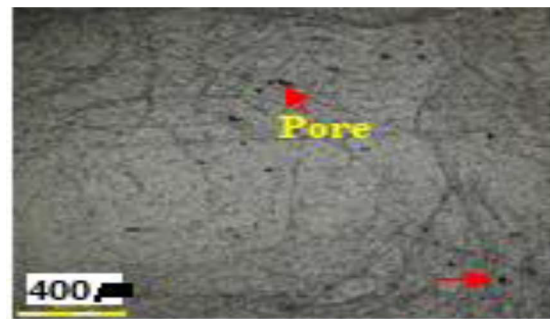


(c) 3 Dimension

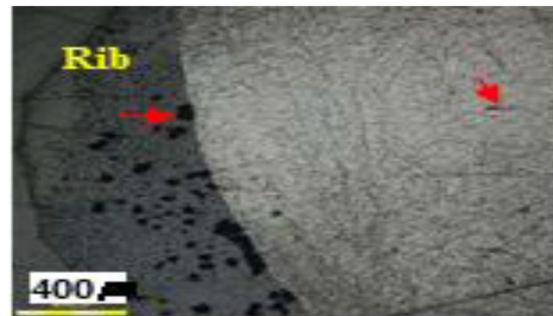
Figure 4. X-ray CT image of No.2 CFRP rebar

words, the pore size and porosity of CFRP rebars were estimated to change depending on the manufacturing method (resin impregnation bath temperature, curing furnace temperature, and holding time).

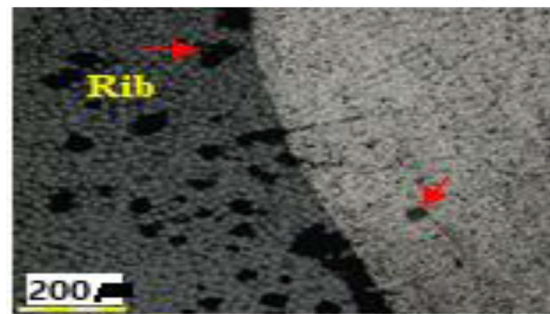
Optical microscopy was used to analyze the porosity of the CFRP rebar cross-sections. Cross-sectional photographs were taken with an optical microscope, and pore characteristics were analyzed using an image analysis program (Olympus DSX). Pore analysis using the DSX program was performed by fixing the pore image color value and activating the pore image for analysis. Figure 5 shows a cross-section of a No. 2 CFRP rebar, in which pores, carbon fibers, and glass fibers can be observed in the cross-section of the CFRP



(a) Main rebar region (Scale Bar 400 μm)



(b) Main rebar + Rib (Scale Bar 400 μm)



(c) Main rebar + Rib (Scale Bar 200 μm)



(d) Main rebar + Rib (Scale Bar 50 μm)

Figure 5. Optical microscope image of No. 2 CFRP rebar

rebar. A small amount of pores were observed in the center of the CFRP rebar as shown in Figure 5(a), while a large number of giant pores were observed in the rib region as shown in Figure 5(b) to 5(d).

Table 4. Porosity obtained by optical microscope

No.	1	2	3	4	5	6	7
Porosity (%)	6.89	5.02	6.64	6.51	5.12	5.24	2.88

The carbon fiber diameter was around 6.5 μm, while the diameter of the glass fiber used as a rib was observed to be around 20 μm. As mentioned in the Nano X-ray CT analysis, the ribs are not resin coated, which explains the large number of macropores observed, and it was assumed that some of the carbon fiber coating resin was absorbed into the glass fiber composite ribs. To analyze the porosity in the CFRP rebar cross-section, image deformation was performed as shown in **Figure 6**, and the white areas after image deformation were considered as pores as shown in **Figure 6(b)**. The calculated porosity values are shown in **Table 4**, and the maximum porosity was 6.89% for No. 1 and the minimum porosity was 2.88% for No. 7. In addition, the porosity derived from optical microscopy was estimated to change with curing temperature conditions, resin impregnation bath temperature, and holding time.

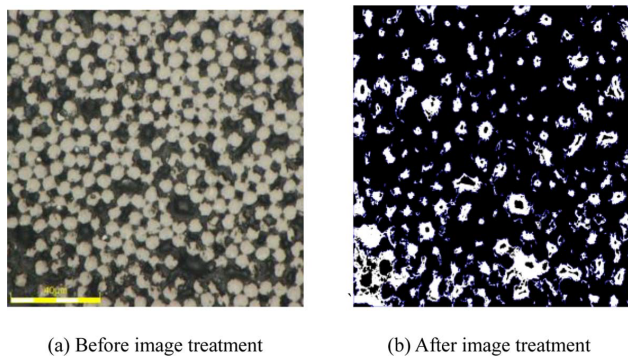
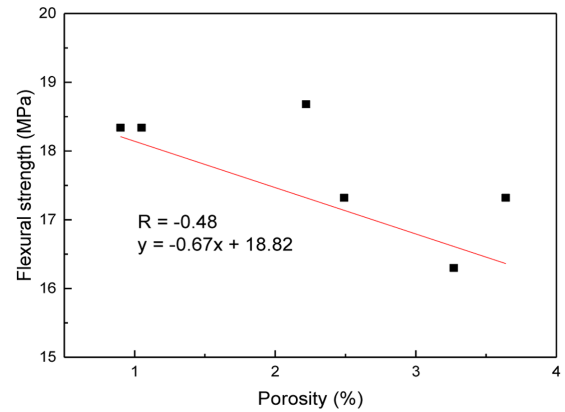


Figure 6. Image process for porosity of No. 4 CFRP rebar

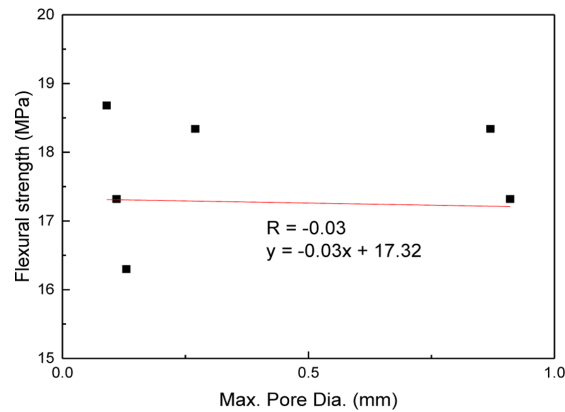
3.3. Flexural strength characterization

The correlation between porosity and flexural strength obtained by X-ray CT of CFRP rebar is shown in **Figure 7**. The correlation coefficient (R) between porosity and flexural strength was -0.48, and the correlation equation was $y = -0.67x + 18.82$ ($y =$ flexural strength, $x =$ porosity). The correlation coefficient between maximum pore diameter and

flexural strength was -0.03, and the correlation equation was $y = -0.03x + 17.32$ ($y =$ flexural strength, $x =$ maximum pore diameter). In general, the correlation coefficient (absolute value) is expressed as 1–0.7 strong linear relationship, 0.7–0.3 clear linear relationship, and 0.3–0.1 weak linear relationship [21]. Therefore, it can be evaluated that porosity and flexural strength have a clear linear relationship, and maximum pore diameter and flexural strength have a weak linear relationship. Therefore, in this study, it can be confirmed that porosity can have some effects on flexural strength, but maximum pore diameter does not have a significant effect on flexural strength.



(a) Porosity and flexural strength



(b) Max. Pore dia. and flexural strength

Figure 7. Correlation between pore characteristics by X-ray CT and flexural strength

The correlation between porosity and flexural strength analyzed using optical microscopy is shown in **Figure 8**, and their correlation coefficient was calculated to be -0.64. In other words, the correlation between porosity and flexural strength using optical microscopy is a clear linear relationship, which is also significantly higher than that using Nano X-ray CT.

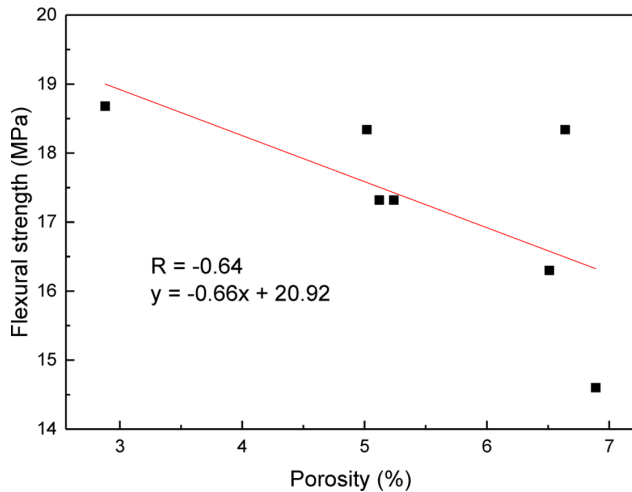


Figure 8. Correlation between pore characteristics by optical microscope and flexural strength

In other words, the correlation between flexural strength and porosity was found to be more valid when analyzed using optical microscopy than Nano X-ray CT. This was due to the fact that finer pores could be observed under optical microscopy (scale bar 40 μm) compared to under Nano X-ray CT (scale bar 800–500 μm), and the difference in porosity between the two methods was very large. In particular, the porosity was significantly higher using the optical microscope, which is easier to observe micropores than Nano X-ray CT, because there are relatively more tens of microscopic pores in CFRP rebars than hundreds of microscopic pores. Therefore, it can be assumed that the flexural strength of CFRP rebars is more dependent on tens of microscopic pores with a large amount of pores.

4. Conclusion

In this study, the flexural strength of CFRP rebars was measured according to the manufacturing conditions,

and the pore characteristics were analyzed by Nano X-ray CT and optical microscopy. The correlation coefficients between the pore properties and the flexural strength obtained by these analytical instruments were also calculated, and the following conclusions were drawn.

- (1) The flexural strength of CFRP rebars varied depending on the manufacturing conditions, including the presence or absence of ribs, curing temperature, curing time, and resin impregnation bath temperature. In particular, it was found that the flexural strength value of the CFRP bar was significantly reduced when the rib was not wrapped.
- (2) It was determined that the pores present in the CFRP rebar were caused by the absorption of the resin from the main reinforcement impregnated with resin by the non-resin impregnated ribs, or the carbon fibers were not perfectly bonded, resulting in residual pores between the fibers.
- (3) Nano X-ray CT analysis showed the maximum pore diameter in CFRP rebars with a resin impregnation bath temperature of 60°C, which was predicted to be due to some curing phenomenon after the CFRP rebars passed through the resin impregnation bath (before entering the curing furnace), i.e., the resin cured rapidly from the time of entering the curing furnace, and the giant pores inside the CFRP rebars were not removed.
- (4) The correlation coefficient of porosity and flexural strength through optical microscopy was -0.64, which was much higher than the correlation coefficient of porosity and pore size through Nano X-ray CT. Therefore, the analysis of micropores through optical microscopy was considered an important factor for predicting and evaluating the flexural strength of CFRP rebar.

Funding

This research was funded by the Ministry of Land, Infrastructure, and Transport, Korea Agency for Infrastructure Technology Advancement (MOLIT) through the Reinforcement Rebar Replacement Material Technology Development Project with Carbon Polymer Corrosion Agent (Grant 22CFRP-C163388-02).

Disclosure statement

The authors declare no conflict of interest.

References

- [1] Lou T, Li Z, Pang M, 2022, Behavior of Externally Prestressed Continuous Beams with FRP/Steel Rebars under Symmetrical/Unsymmetrical Loading: Numerical Study. *Case Studies in Construction Materials*, 2022(17): e01196.
- [2] Benghida D, 2017, Concrete as a Sustainable Construction Material. *Key Engineering Materials*, 2017(744): 196–200.
- [3] Gu JB, Wang JY, Lu W, 2022, An Experimental Assessment of Ultra High Performance Concrete Beam Reinforced with Negative Poisson's Ratio Steel Rebar. *Construction and Building Materials*, 2022(327): 127042.
- [4] Fan L, Teng L, Tang F, et al., 2021, Corrosion of Steel Rebar Embedded in UHPC Beams with Cracked Matrix. *Construction and Building Materials*, 2021(313): 125589.
- [5] Dong B, Liu W, Zhang T, et al., 2021, Corrosion Failure Analysis of Low Alloy Steel and Carbon Steel Rebar in Tropical Marine Atmospheric Environment: Outdoor Exposure and Indoor Test. *Engineering Failure Analysis*, 2021(129): 105720.
- [6] Choi JS, Park SJ, Kim YH, 2021, Comparison of Mechanical Properties on Helical/Hoop Hybrid Wound HNT Reinforced CFRP Pipe with Water Absorption Behavior. *Composites Research*, 34(3): 174–179.
- [7] Çelik A, Lazoglu I, Kara A, et al., 2015, Investigation on the Performance of SiAlON Ceramic Drills on Aerospace Grade CFRP Composites. *Journal of Materials Processing Technology*, 2015(223): 39–47.
- [8] Kim KS, Shim YS, Kim BJ, et al., 2010, Present Status and Applications of Carbon Fibers-Reinforced Composites for Aircrafts. *Carbon Letters*, 2010(11): 235–242.
- [9] Hong CS, Jun WJ, 1984, Fiber Reinforced Composite Material Application for Light Airplane. *Journal of the Korean Society for Aeronautical & Space Sciences*, 12(2): 3–8.
- [10] Slayton R, Spinardi G, 2016, Radical Innovation in Scaling up: Boeing's Dreamliner and the Challenge of Socio-Technical Transitions. *Technovation*, 2016(47): 47–58.
- [11] Stig F, 2009, An Introduction to the Mechanics of 3D-Woven Fibre Reinforced Composites. thesis, KTH Engineering Sciences.
- [12] Yoon CM, Lee DW, Byun JH, et al., 2022, Study on Out-of-plane Properties and Failure Behavior of Aircraft Wing Unit Structures. *Composites Research*, 35(2): 106–114.
- [13] Attia MM, Ahmed O, Kobesy O, et al., 2022, Behavior of FRP Rod Under Uniaxial Tensile Strength with Multiple Materials as an Alternative to Steel Rebar. *Case Studies in Construction Materials*, 2022(17): e01241.
- [14] Li T, Zhu H, Shen J, et al., 2022, Thermophysical and Thermomechanical Properties of Basalt-Phenolic FRP Rebars

- Under High Temperature. *Construction and Building Materials*, 2022(342): 127983.
- [15] Huang L, Chen J, Qu J, et al., 2020, Modeling for Bond-Constitutive Relationship of FRP Rebars to Concrete Matrix. *Construction and Building Materials*, 2020(263): 120654.
- [16] Abbas EMA, Ge Y, Zhanag Z, et al., 2022, Flexural Behavior of UHPC Beam Reinforce with Steel-FRP Composite Bars. *Case Studies in Construction Materials*, 2022(16): e01110.
- [17] Cao X, Ren Y, Zhanag L, et al., 2022, Flexural Behavior of Ultra High Performance Concrete Beams with Various Types of Rebar. *Composite Structures*, 2022(292): 115674.
- [18] Abbas H, Abadel A, Almusallam T, et al., 2022, Experimental and Analytical Study of Flexural Performance of Concrete Beams Reinforced with Hybrid of GFRP and Steel Rebars. *Engineering Failure Analysis*, 2022(138): 106397.
- [19] Ge W, Han MY, Guan Z, et al., 2021, Tension and Bonding Behavior of Steel-FRP Composite Bars Subjected to the Coupling Effects of Chloride Corrosion and Load. *Construction and Building Materials*, 2021(296): 123641.
- [20] Kim HS, Kim WJ, Jang HS, et al., 2010, A Study on the Change of Strength of FRP Member Immersed in Chemical Solution. *Korea Institute for Structural Maintenance and Inspection*, 14(6): 117–123.
- [21] Wikipedia homepage, <http://ko.wikipedia.org> > wiki > correlation analysis.

Publisher's note:

Art & Technology Publishing remains neutral with regard to jurisdictional claims in published maps and institutional affiliations.